Single/multiple-mode-selection optical nanofilters based on end-coupled split-ring resonators

Kunhua Wen,[1,*] Yihua Hu,[1] Li Chen,[1] Liang Lei,[1] and Zhen Guo[2,3]

[1]School of Physics and Optoelectronic Engineering, Guangdong University of Technology, Guangzhou 510006, China

[2]School of Information Science and Technology, Southwest Jiaotong University, Chengdu 610031, China

[3]State Key Laboratory of Optical Technologies for Microfabrication, Chinese Academy of Science, Chengdu 610029, China

*Corresponding author: khwen@gdut.edu.cn

Received 19 February 2014; revised 10 May 2014; accepted 14 May 2014;
posted 20 May 2014 (Doc. ID 206798); published 23 June 2014

A plasmonic mode-selection filter based on end-coupled circular split-ring resonators is proposed and demonstrated. In contrast to regular ring resonators, which can support only the integer modes, extra noninteger resonance modes will be excited by placing metallic nanowalls in the proposed circular ring resonators. Since all the modes are highly sensitive to the position of the nanowall, the associated modes are effectively excited or suppressed by manipulating the position. This proposed scheme offers great flexibility to design the transmission spectrum with expected modes. Moreover, each integer or noninteger resonance mode with high transmittance can be selected individually by cascading two proposed split-ring resonators that share an intersection of transmission peaks. The corresponding spectra and the propagation characteristics are numerically investigated by using the finite-difference time-domain method.

OCIS codes: (240.6680) Surface plasmons; (130.3120) Integrated optics devices; (230.4555) Coupled resonators.

http://dx.doi.org/10.1364/AO.53.004158

1. Introduction

As surface plasmon polaritons (SPPs) have been considered one of the most promising ways to overcome the diffraction limit of optical waves, they are mostly preferred in developing highly integrated photonic circuits. Recently, great effort has been made to study the characteristics of various nanoscale/microscale structures [1,2], such as particles [3,4], grooves [5–8], cavities or equivalent cavities [9–14], and apertures [15–17]. Among those subwavelength structures, metal–insulator–metal (MIM) waveguides show many potential applications in the optical information area, because of their advantages of easy fabrication and strong light confinement. Accordingly, many MIM-based devices have been designed and demonstrated, such as Mach–Zehnder interferometers [18], Y-shaped combiners [19], couplers [20,21], and circulators [22,23]. Conventionally, long-range propagation for SPPs in MIM waveguides is preferred. Meanwhile, more attention is paid to their spectral responses, as the wavelength-selection performance including passband and stopband are desired in many optical systems. Specifically, photonic bandgaps are achieved in a MIM structure consisting of periodic insulators or grooves [24–28]. In addition, side-coupled or end-coupled slot cavities, which act as resonators, are also proposed to obtain multiple transmission/reflection channels [29–31]. Another type of resonators with similar performance is the closed rings with circular or rectangular geometries [32–37], which are used as an add–drop coupler as well. However, the wavelengths of resonance modes in these optical MIM filters are usually proportional to the length of the resonators.

1559-128X/14/194158-06$15.00/0

In this paper, a single-/multiple-mode-selection optical nanofilter based on end-coupled split-ring resonators (SRRs) is proposed. Since one or two nanowalls are positioned inside a MIM circular ring, either the noninteger or the integer resonance modes can be significantly suppressed or excited. More importantly, unlike those integer modes, the noninteger ones cannot be achieved by using the regular closed ring directly and they are highly sensitive to the nanowall positions. Next, by cascading two SRRs with specified nanowall locations, one can separate all the expected noninteger or integer modes in a large wavelength range. Then the finite-difference time-domain (FDTD) method with perfectly matched layer (PML) boundary conditions is used to demonstrate the desired characteristics of the proposed filter.

2. Theory and Analysis

Figure 1 shows the schematic diagram of the proposed structure, where the metal and the insulator are assumed to be silver and air, respectively. The circular SRR is located between two MIM waveguides with a coupling distance of s. Due to the symmetry of the structure, the position of the nanowall is defined as the angle (i.e., φ) between the nanowall and the y-axis direction in a quarter-circle range, as shown in Fig. 1(a). In other words, the condition of $0° \le \varphi \le 90°$ is satisfied, as denoted in Figs. 1(c)–1(i). In the following simulations and analyses, φ is used to distinguish the position of the nanowall.

Before analysis of the characteristics of the SRR, the resonance phase condition of the closed ring without defect [see Fig. 1(b)] is given first, as

$$k\,\mathrm{Re}(n_{\mathrm{eff}})L_{\mathrm{eff}} + \Delta\theta = 2m\pi, \qquad m = 1, 2, 3, \ldots, \quad (1)$$

where m stands for the integer resonance mode, $L_{\mathrm{eff}} = \pi(R + r)$ is the equivalent resonant length, r and R are the inner radius and outer radius, respectively, $k = 2\pi/\lambda_m$ is the free-space wave vector, $\Delta\theta$ is the phase change due to the reflection at the resonator facet, and $\mathrm{Re}(n_{\mathrm{eff}})$ is the real part of the effective index n_{eff}, which can be obtained from the dispersion equation of the TM mode in the waveguide given by [38]:

$$\varepsilon_i k_m + \varepsilon_m k_i \tanh(-jk_i W/2) = 0. \quad (2)$$

Here, $k_{i,m} = \sqrt{\varepsilon_{i,m}k_0^2 - \beta^2}$ are the transverse propagation constants in air and silver, respectively, W is the width of the waveguide, and ε_i and ε_m are the permittivities of air and silver, respectively. The propagation constant, $\beta = k_0 n_{\mathrm{eff}}$, is represented as a function of the effective index of the waveguide.

From Eq. (1), it is known that the integer resonance modes in the closed MIM circular ring are dependent mainly on the length of the resonator. Typically, a close relationship between the center wavelengths of the resonance modes can be specified as $\lambda_1 : \lambda_2 = 1 : 1/2$, where λ_1 and λ_2 are the center wavelengths of the first and the second modes (i.e., TM_1 and TM_2), respectively. However, the integer modes will be interrupted through splitting the ring with a metallic nanowall that locates at the nodes or antinodes of the magnetic field. Thus, the magnetic field distributions in the resonator are completely destructed and rearranged, based on which the resonance modes, including the integer modes or noninteger mode, may be suppressed or excited. Note that, for the new generated noninteger modes, such as TM_n, the resonance phase condition in Eq. (1) no longer holds. Here, $n = (2m + 1)/2$ and m is an integer.

To calculate the transmittance and to analyze the electromagnetic responses, a frequency-domain power or profile is placed at position Q to record the magnetic fields $H(\omega)$ and the electric fields $E(\omega)$. Consequently, the complex Poynting vector $\vec{P} = \vec{E}(\omega) \times \vec{H}^*(\omega)$ at the specific frequencies can be obtained immediately, and then the time-averaged power flowing through a surface can be calculated as $\mathrm{Power}(\omega) = [\int \mathrm{real}(\vec{P}) \cdot d\vec{s}]/2$.

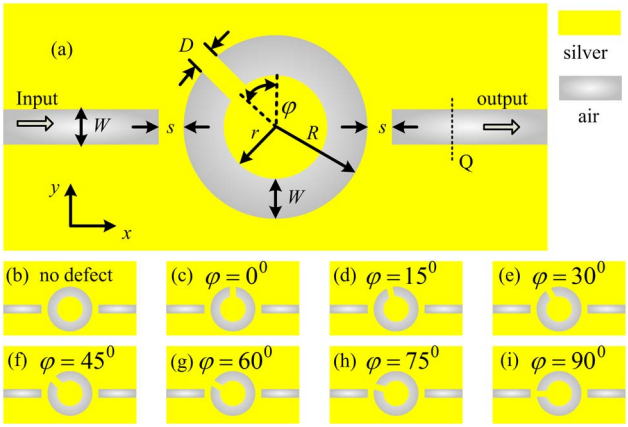

Fig. 1. Schematic diagram of the proposed plasmonic filter based on the SRR structure (a) including a metallic nanowall, (b) without defect, and (c)–(i) including a nanowall with angles from 0° to 90°.

3. Simulations and Discussion

During the simulations using FDTD, the parameters are defined as: the width of the nanowall $D = 20$ nm, the coupling distance $s = 10$ nm, the inner radius $r = 150$ nm, the outer radius $R = 200$ nm, and the width of the waveguide $W = 50$ nm. Moreover, the tabulation of the optical constants of silver in Ref. [39] is used. Figure 2(a) shows the transmission spectrum of the resonator without nanowalls. Obviously, there are no transmission peaks in the wavelength range from 600 to 1800 nm, except for the integer resonance modes of TM_1 at 1568 nm and TM_2 at 793 nm. An even number of antinodes can be found in the magnetic field distributions, as shown in the insets of Fig. 2(a). Then, a nanowall with an angle φ is embedded into the ring. Such an angle increases from 0° to 90° with a step of 15°, as shown in the insets of Figs. 2(b)–2(h). In Fig. 2(b), two extra resonance

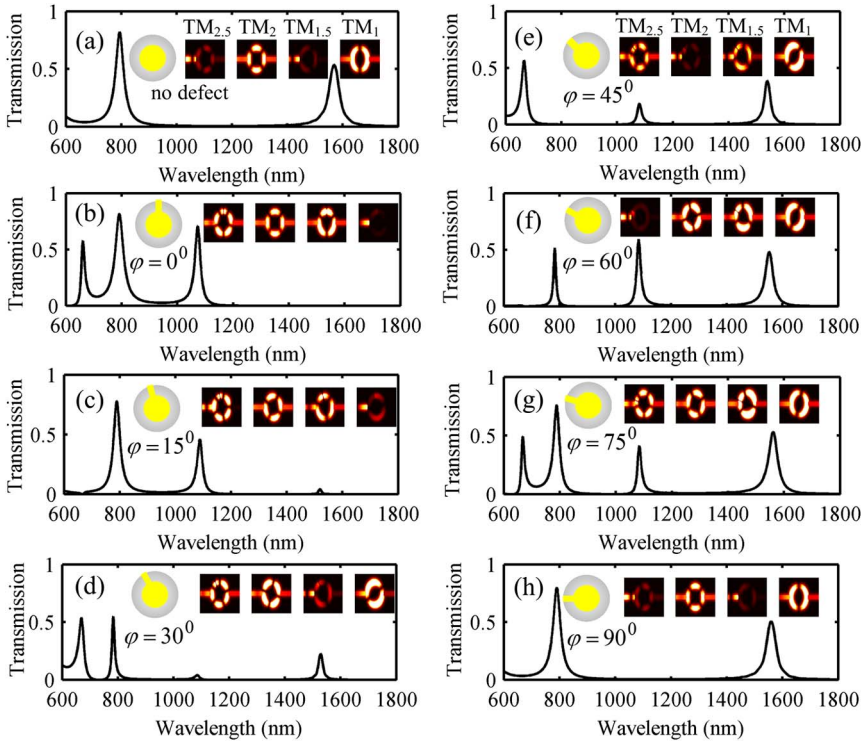

Fig. 2. Transmission spectra of the circular ring (a) without defect, and (b)–(h) with a nanowall whose angle φ increases from 0° to 90°. The insets are the schematic of the SRR and the magnetic-field distributions at the resonance wavelengths.

modes arise between modes TM_1 and TM_2, or between modes TM_2 and TM_3, and they are named $TM_{1.5}$ at 1073 nm and $TM_{2.5}$ at 661 nm. TM_1 is completely suppressed because the nanowall with $\varphi = 0°$ is placed at the antinode of its magnetic field intensity. Meanwhile, TM_2 remains at the same wavelength as that in Fig. 2(a). The magnetic field distributions of TM_1, $TM_{1.5}$, TM_2, and $TM_{2.5}$ can be found in the insets of Fig. 2(b), indicating that $TM_{1.5}$, TM_2, and $TM_{2.5}$ can pass through the MIM waveguide, while TM_1 will be stopped. Interestingly, there are odd-number antinodes for the magnetic field of the noninteger resonance modes of $TM_{1.5}$ and $TM_{2.5}$, which is different from that of TM_1 and TM_2.

In the following simulations, the nanowall is positioned at other positions with $\varphi = 15°$, 30°, 45°, 60°, 75°, and 90°. The resulting transmission spectra and the resonance mode profiles of the magnetic field are shown in Figs. 2(c)–2(h). It is obvious that the generated integer or noninteger modes supported in the SRR are greatly changed by adjusting the position of the nanowall. For easy analysis, all the simulation results are listed in Table 1 with detailed transmittances of the excited/suppressed resonance modes.

From Table 1, one can easily obtain the corresponding states of the integer or noninteger modes for different φ. Specifically, the supported modes are $TM_{1.5}$, TM_2, and $TM_{2.5}$ in Fig. 1(b); $TM_{1.5}$ and TM_2 in Fig. 1(c); TM_1, TM_2, and $TM_{2.5}$ in Fig. 1(d); TM_1, $TM_{1.5}$, and $TM_{2.5}$ in Fig. 1(e); TM_1, $TM_{1.5}$, and TM_2 in Fig. 1(f); TM_1, $TM_{1.5}$, TM_2, and $TM_{2.5}$ in Fig. 1(g); and TM_1 and TM_2 in Fig. 1(h).

In order to clarify more details about the effect of the SRR, dual nanowalls in a line are used to separate the circular ring into two equivalent parts, as shown in Fig. 3(a). In view of the SPP field skin depth (less than 30 nm [27]) in metal, the width of the nanowalls is defined as 5 nm to avoid complete suppression of SPP propagation, and the spacing between two SRRs is set as 15 nm. The other parameters are identical to those in Fig. 2 during simulation using FDTD. The obtained transmission spectra are presented in Figs 3(b)–3(g). Likewise, noninteger resonance modes can also be achieved via the dual-nanowalls arrangement. However, even with the same angle φ, the supported modes in the SRRs with two nanowalls are different from those in the SRR with one nanowall. For example, the modes in

Table 1. Transmittances of Resonant Modes with Different Positions of Nanowalls

	T			
φ	TM_1	$TM_{1.5}$	TM_2	$TM_{2.5}$
No nanowall	0.54	0.01	0.82	0.04
0°	0.00	0.70	0.82	0.58
15°	0.04	0.46	0.78	0.00
30°	0.23	0.04	0.55	0.54
45°	0.38	0.18	0.00	0.56
60°	0.48	0.59	0.52	0.00
75°	0.53	0.41	0.76	0.49
90°	0.50	0.00	0.80	0.04

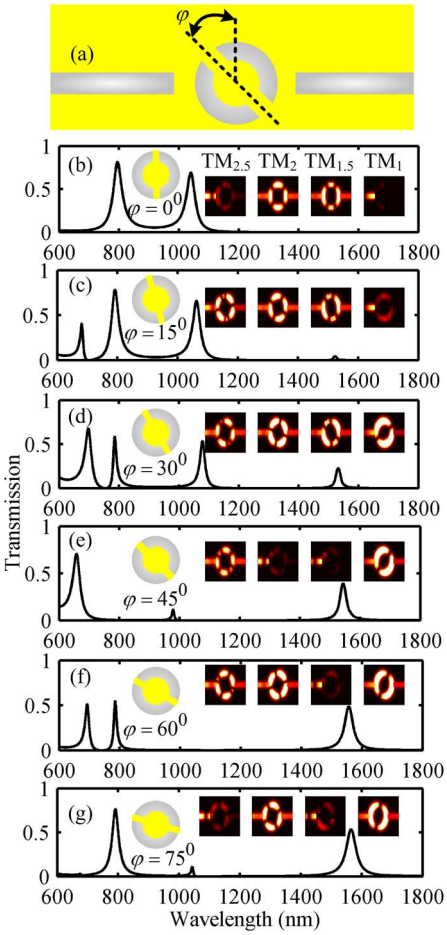

Fig. 3. Transmission spectra of the SRR with dual nanowalls in a line. The insets illustrate the schematic of the SRR and the magnetic-field distributions at the resonance wavelengths.

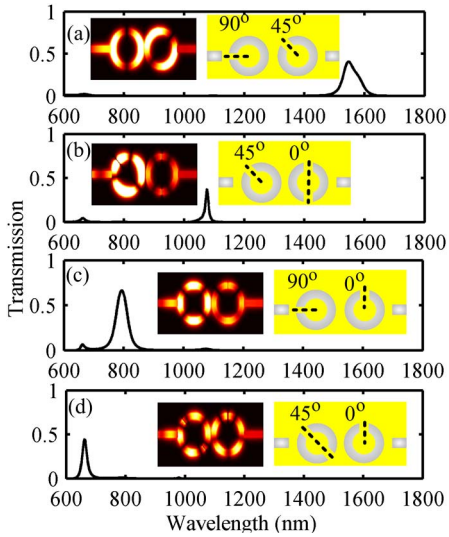

Fig. 4. Transmission spectra of the separated modes by cascading two SRRs: (a) TM_1, (b) $TM_{1.5}$, (c) TM_2, and (d) $TM_{2.5}$. The insets are the schematics of the SRR and the magnetic-field distributions at the resonance wavelengths.

Table 2. Transmittances and Wavelengths for Each Mode

Modes	TM_1	$TM_{1.5}$	TM_2	$TM_{2.5}$
λ (nm)	1546	1076	793	662
T	0.41	0.38	0.66	0.45

Fig. 3(b) are $TM_{1.5}$ and TM_2, while those in Fig. 2(b) are $TM_{1.5}$, TM_2, and $TM_{2.5}$ in the case of $\varphi = 0°$. The excited modes are $TM_{1.5}$, TM_2, and $TM_{2.5}$ in Fig. 3(c); TM_1, $TM_{1.5}$, TM_2, and $TM_{2.5}$ in Fig. 3(d); TM_1 and $TM_{2.5}$ in Fig. 3(e); TM_1, TM_2, and $TM_{2.5}$ in Fig. 3(f); and TM_1 and TM_2 in Fig. 3(g).

Interestingly, each integer or noninteger resonance mode can be separated by cascading two SRRs. Comparing the transmission peaks in Fig. 2 with those in Fig. 3, the intersection mode for two specific resonators can pass through the MIM waveguide, while other modes will be suppressed again. Specifically, (i) the same mode supported in the SRR with a 90°-positioned nanowall and the one with a 45°-positioned nanowall is TM_1, (ii) the same mode supported in the SRR with a 45°-positioned nanowall and the one with two 0°-positioned nanowalls is $TM_{1.5}$, (iii) the same mode supported in the SRR with a 90°-positioned nanowall and the SRR with a 0°-positioned nanowall is TM_2, and (iv) the same mode supported in the SRR with a 0°-positioned nanowall and the SRR with two 45°-positioned nanowalls is $TM_{2.5}$. Therefore, all the modes can be obtained individually by cascading the two mentioned resonators with different nanowall arrangements, and an array of such arrangements can be used for optical/microwave channelization [40]. The obtained spectra in Fig. 4 clearly show that there is only a single transmission peak in the wavelength range from 600 to 1800 nm for each arrangement. This feature is completely different from those in Figs. 2 and 3. The transmittances and the wavelengths for the separated modes of TM_1, $TM_{1.5}$, TM_2, and $TM_{2.5}$ are shown in Table 2. In addition, more details can be found in the insets, which illustrate the magnetic field distribution for each mode. This proposed structure might find applications requiring a single passband in transmission responses. In this paper, we focus mainly on the 2D FDTD simulation. The coupling loss in a 3D model is a little larger than that in a 2D case, and thus the transmittance will be reduced. However, similar results are expected in the 3D model with comparable accuracy based on our previous results, but take much more time [12,41].

4. Conclusion

In summary, a mode-selection SRR filter based on a MIM waveguide has been proposed. In addition to the integer resonance modes, specific noninteger modes, which could not be obtained in a regular ring resonator, were achieved by placing one or two nanowalls in the end-coupled ring resonators. The simulation results based on the FDTD method

demonstrated that the position of the nanowall significantly affected the characteristics of the resonance modes, which made the filter design more flexible and the resonance wavelength tunable. In addition, based on the intersection modes of two SRRs. each integer and noninteger mode could be separated. This kind of SRR filter might find wide applications in integrated optical circuits and optical systems.

The work was supported by the China Postdoctoral Science Foundation (No. 2014M552173), the Research Fund of Guangdong University of Technology, and the Open Research Fund of the State Key Laboratory of Optical Technologies for Micro-Engineering and Nano-Fabrication of China.

References

1. C. Zhang, R. Wang, Y. Wang, S. Zhu, C. Min, and X. C. Yuan, "Phase-stepping technique for highly sensitive microscopic surface plasmon resonance biosensor," Appl. Opt. **53**, 836–840 (2014).
2. H. Fan and P. Berini, "Thermo-optic characterization of long-range surface-plasmon devices in Cytop," Appl. Opt. **52**, 162–170 (2013).
3. S. A. Maier, P. G. Kik, H. A. Atwater, S. Meltzer, E. Harel, B. E. Koel, and A. G. Requicha, "Local detection of electromagnetic energy transport below the diffraction limit in metal nanoparticle plasmon waveguides," Nat. Mater. **2**, 229–232 (2003).
4. W. H. Weber and G. W. Ford, "Propagation of optical excitations by dipolar interactions in metal nanoparticle chains," Phys. Rev. B **70**, 125409 (2004).
5. S. I. Bozhevolnyi, V. S. Volkov, E. Devaux, and T. W. Ebbesen, "Channel plasmon-polariton guiding by subwavelength metal grooves," Phys. Rev. Lett. **95**, 046802 (2005).
6. X. S. Lin and X. G. Huang, "Tooth-shaped plasmonic waveguide filters with nanometric sizes," Opt. Lett. **33**, 2874–2976 (2008).
7. C. T. Wang, C. L. Du, Y. G. Lv, and X. G. Luo, "Surface electromagnetic wave excitation and diffraction by subwavelength slit with periodically patterned metallic grooves," Opt. Express **14**, 5671–5681 (2006).
8. K. H. Wen, L. S. Yan, W. Pan, B. Luo, Z. Guo, Y. H. Guo, and X. G. Luo, "Spectral characteristics of plasmonic metal-insulator-metal waveguides with a tilted groove," IEEE Photon. J. **4**, 1794–1800 (2012).
9. Q. Zhang, X. G. Huang, X. S. Lin, J. Tao, and X. P. Jin, "A subwavelength coupler-type MIM optical filter," Opt. Express **17**, 7549–7554 (2009).
10. J. C. Weeber, A. Bouhelier, F. G. Des, L. Markey, and A. Dereux, "Submicrometer in-plane integrated surface plasmon cavities," Nano Lett. **7**, 1352–1359 (2007).
11. F. F. Hu, H. X. Yi, and Z. P. Zhou, "Wavelength demultiplexing structure based on arrayed plasmonic slot cavities," Opt. Lett. **36**, 1500–1502 (2011).
12. K. H. Wen, L. S. Yan, W. Pan, B. Luo, Z. Guo, and Y. H. Guo, "Wavelength demultiplexing structure based on plasmonic metal-insulator-metal waveguide," J. Opt. **14**, 075001 (2012).
13. K. H. Wen, L. S. Yan, W. Pan, B. Luo, Z. Guo, and Y. H. Guo, "Design of plasmonic comb-like filters using loop-based resonators," Plasmonics **8**, 1017–1022 (2013).
14. X. Zou, M. Li, W. Pan, L. Yan, J. Azaña, and J. Yao, "All-fiber optical filter with an ultra-narrow and rectangular spectral response," Opt. Lett. **38**, 3096–3098 (2013).
15. Y. Yang, H. T. Dai, and X. W. Sun, "Split ring aperture for optical magnetic field enhancement by radially polarized beam," Opt. Express **21**, 6845–6850 (2013).
16. S. S. Walavalkar, P. Latawiec, A. Homyk, and A. Scherer, "Scalable method for the fabrication and testing of glass filled, three-dimensionally sculpted extraordinary transmission apertures," Nano Lett. **14**, 311–317 (2014).
17. P. A. Brandão and S. B. Cavalcanti, "Optical spin-to-orbital plasmonic angular momentum conversion in subwavelength apertures," Opt. Lett. **38**, 920–922 (2013).
18. S. I. Bozhevolnyi, V. S. Volkov, E. Devaux, J. Y. Laluet, and T. W. Ebbesen, "Channel plasmon subwavelength waveguide components including interferometers and ring resonators," Nature **440**, 508–511 (2006).
19. H. Gao, H. Shi, C. Wang, C. Du, X. Luo, Q. Deng, Y. Lv, X. Lin, and H. Yao, "Surface plasmon polariton propagation and combination in Y-shaped metallic channels," Opt. Express **13**, 10795–10800 (2005).
20. T. W. Lee and S. Gray, "Subwavelength light bending by metal slit structures," Opt. Express **13**, 9652–9659 (2005).
21. R. A. Wahsheh, Z. Lu, and M. A. G. Abushagur, "Nanoplasmonic couplers and splitters," Opt. Express **17**, 19033–19040 (2009).
22. K. H. Wen, L. S. Yan, W. Pan, B. Luo, Z. Guo, and Y. H. Guo, "A four-port plasmonic quasi-circulator based on metal-insulator-metal waveguides," Opt. Express **20**, 28025–28032 (2012).
23. M. A. Bavil, Z. Zhou, and Q. Deng, "Active unidirectional propagation of surface plasmons at subwavelength slits," Opt. Express **21**, 17066–17076 (2013).
24. A. Pannipitiya, I. D. Rukhlenko, M. Premaratne, H. T. Hattori, and G. P. Agrawal, "Improved transmission model for metal-dielectric-metal plasmonic waveguides with stub structure," Opt. Express **18**, 6191–6204 (2010).
25. J. Tao, X. G. Huang, X. S. Lin, Q. Zhang, and X. P. Jin, "A narrow-band subwavelength plasmonic waveguide filter with asymmetrical multiple-teeth-shaped structure," Opt. Express **17**, 13989–13994 (2009).
26. Z. H. Han, E. Forsberg, and S. L. He, "Surface plasmon Bragg gratings formed in metal-insulator-metal waveguides," IEEE Photon. Technol. Lett. **19**, 91–93 (2007).
27. B. Wang and G. P. Wang, "Plasmon Bragg reflectors and nanocavities on flat metallic surfaces," Appl. Phys. Lett. **87**, 013107 (2005).
28. X. Luo, X. H. Zou, X. F. Li, Z. Zhou, W. Pan, L. S. Yan, and K. H. Wen, "High-uniformity multichannel plasmonic filter using linearly lengthened insulators in metal-insulator-metal waveguide," Opt. Lett. **38**, 1585–1587 (2013).
29. G. Wang, H. Lu, X. Liu, D. Mao, and L. Duan, "Tunable multichannel wavelength demultiplexer based on MIM plasmonic nanodisk resonators at telecommunication regime," Opt. Express **19**, 3513–3518 (2011).
30. H. Lu, X. Liu, D. Mao, L. Wang, and Y. Gong, "Tunable band-pass plasmonic waveguide filters with nanodisk resonators," Opt. Express **18**, 17922–17927 (2010).
31. Y. H. Guo, L. S. Yan, W. Pan, B. Luo, K. H. Wen, Z. Guo, H. Li, and X. G. Luo, "A plasmonic splitter based on slot cavity," Opt. Express **19**, 13831–13838 (2011).
32. A. Hosseini and Y. Massoud, "Nanoscale surface plasmon based resonator using rectangular geometry," Appl. Phys. Lett. **90**, 181102 (2007).
33. T. B. Wang, X. W. Wen, C. P. Yin, and H. Z. Wang, "The transmission characteristics of surface plasmon polaritons in ring resonator," Opt. Express **17**, 24096–24101 (2009).
34. T. Holmgaard, Z. Chen, S. I. Bozhevolnyi, L. Markey, and A. Dereux, "Dielectric-loaded plasmonic waveguide ring resonators," Opt. Express **17**, 2968–2975 (2009).
35. B. Yun, G. Hu, and Y. Cui, "Theoretical analysis of a nanoscale plasmonic filter based on a rectangular metal-insulator-metal waveguide," J. Phys. D **43**, 385102 (2010).
36. F. S. Ma and C. Lee, "Optical nanofilters based on meta-atom side-coupled plasmonics metal-insulator-metal waveguides," J. Lightwave Technol. **31**, 2876–2880 (2013).
37. I. Zand, M. S. Abrishamian, and P. Berini, "Highly tunable nanoscale metal-insulator-metal split ring core ring resonators (SRCRRs)," Opt. Express **21**, 79–86 (2013).
38. J. A. Dionne, L. A. Sweatlock, and H. A. Atwater, "Plasmon slot waveguides: towards chip-scale propagation with

subwavelength-scale localization," Phys. Rev. B **73**, 035407 (2006).
39. P. B. Johnson and R. W. Christy, "Optical constants of the noble metals," Phys. Rev. B **6**, 4370–4379 (1972).
40. X. Zou, W. Li, W. Pan, L. Yan, and J. Yao, "Photonic-assisted microwave channelizer with improved channel characteristics based on spectrum-controlled stimulated Brillouin scattering," IEEE Trans. Microw. Theory Tech. **61**, 3470–3478 (2013).
41. Y. H. Guo, L. S. Yan, W. Pan, B. Luo, K. H. Wen, Z. Guo, and X. G. Luo, "Electromagnetically induced transparency (EIT)-like transmission in side-coupled complementary split-ring resonators," Opt. Express **20**, 24348–24355 (2012).